Review Article

62

INDONESIAN SCHOLAR SOCIETY

Indones. J. Chem. Stud.
2026, 5(1), 62–73
Available online at journal.solusiriset.com
e-ISSN: 2830-7658; p-ISSN: 2830-778X

Indonesian Journal of Chemical Studies

Bismuth Oxide-Based Photocatalytic Nanoplatforms for Cancer Theranostics - Advances, Mechanisms, and Clinical Prospects

Reyhan Natadilandes[1], Wardah Ibnatis Tsaniyah[2], Lathifah Puji Hastuti[1]*, Suseno Amien[1]

[1]*Graduate School, Universitas Padjadjaran, Dipati Ukur Street No. 35, Bandung 40132, Indonesia*

[2]*Faculty of Mathematics, Natural Sciences, and Health, Universitas Muhammadiyah Riau, Tuanku Tambusai Street, Pekanbaru 28290, Indonesia*

Received: 1 Dec 2025; Revised: 9 Apr 2026; Accepted: 13 Apr 2026;
Published online: 30 Jun 2026; Published regularly: 30 Jun 2026

Abstract— The growing demand for precise, minimally invasive, and image-guided cancer management has accelerated the development of multifunctional theranostic platforms capable of unifying diagnosis and therapy. Among emerging inorganic nanomaterials, bismuth oxide (Bi_2O_3) has gained significant attention due to its high atomic number, strong X-ray attenuation, tunable semiconductor band structure, and intrinsically favorable biocompatibility. This review provides a synthesis of advances in Bi_2O_3-based photocatalytic nanoplatforms for cancer theranostics. This article discusses how phase control, defect engineering, doping, and heterojunction construction enable enhanced ROS generation, improved charge separation, broadened optical absorption, and synergistic radiosensitization. These physicochemical features underpin a wide range of theranostic applications, including CT, photoacoustic, and multimodal imaging (photodynamic-, sonodynamic-, and photothermal-type therapies), radiotherapy enhancement; controlled chemotherapy delivery; and emerging immunomodulatory strategies. State-of-the-art designs increasingly integrate hierarchical architectures, oxygen-vacancy engineering, NIR-responsive components, and tumor microenvironment–activated functionalities to achieve intelligent, multi-stimuli cancer treatment. Despite their promise, key translational challenges persist, particularly relating to long-term biodistribution, clearance, standardized manufacturing, and regulatory validation. By consolidating mechanistic insights and engineering principles, this review outlines design guidelines for the rational development of clinically viable Bi_2O_3-based nanoplatforms and highlights their potential to bridge diagnostic imaging with personalized, multi-modal cancer therapy.

Keywords— *Bi_2O_3; Diagnostic; Nanoparticle; Photothermal; Photodynamic; ROS*

1. INTRODUCTION

Cancer remains a leading cause of morbidity and mortality worldwide despite remarkable progress in molecular oncology, targeted agents, and immunotherapies [1]. Conventional cancer treatments like surgery, chemotherapy, and radiotherapy face significant limitations, including off-target toxicity, heterogeneous patient response, and poor drug penetration into the complex tumor microenvironment [2-4]. To address these challenges, the paradigm of "theranostics" has emerged, which integrates diagnostic and therapeutic functions into a single, unified platform. This approach aims to close the loop between tumor visualization, treatment monitoring, and targeted therapy for personalized care [5]. Nanomedicine is pivotal in enabling theranostics, as engin eered nanoparticles can exploit the Enhanced Permeability and Retention (EPR) effect for tumor accumulation, deliver therapeutic payloads, generate reactive oxygen species (ROS), and provide contrast for various imaging modalities [6].

Within nanomedicine, inorganic nanomaterials with high atomic numbers (High-Z) are particularly promising. They simultaneously enhance imaging contrast and amplify therapeutic energy deposition [7]. Among these, bismuth-based nanomaterials stand out due to bismuth's very high atomic number (Z=83), which confers strong X-ray absorption for superior CT contrast and radiosensitization, alongside a relatively favorable biocompatibility profile compared to other heavy metals [8-9].

Bismuth oxide (Bi_2O_3) is a highly compelling form of bismuth that adds a unique photocatalytic capability to these inherent High-Z properties. With a band gap suitable for visible light absorption, Bi_2O_3 can generate electron-hole pairs upon photoexcitation that drive the formation of ROS [10-11]. This photocatalytic activity can be harnessed for cancer therapy, inducing oxidative damage in a manner similar to photodynamic therapy. The unique synergy of Bi_2O_3 lies in its ability to couple this photocatalytic ROS generation with its High-Z functions within a single nanoplatform [12].

Recent advances have led to sophisticated Bi_2O_3 nanostructures like nanorods and nanosheets, engineered for improved theranostic performance. The formation of heterojunctions with other semiconductors

***Corresponding author**.
Email address: Lathifah.puji@unpad.ac.id
DOI: 10.55749/ijcs.v5i1.137

has been especially effective, creating platforms that synergistically combine therapies like sonodynamics, radiotherapy, and chemotherapy [13-14] Parallel efforts in developing biodegradable and polymer-coated Bi_2O_3 agents further highlight the focus on tailoring pharmacokinetics and biosafety for clinical translation [15].

Despite this progress, the literature on Bi_2O_3 remains fragmented, often focusing on its environmental applications or treating it as merely one member of the bismuth family, thereby lacking a dedicated synthesis that bridges its established photocatalytic chemistry with its emerging potential in multimodal cancer theranostics [11,16].

This review comprehensively examines bismuth oxide (Bi_2O_3)-based photocatalytic nanoplatforms for cancer theranostics. It begins by outlining the fundamental properties of Bi_2O_3 that are crucial for photocatalysis and biomedical use. The discussion then covers engineering strategies to optimize these properties for enhanced performance. The core of the review analyzes the mechanisms behind ROS generation, photothermal effects, radiosensitization, and drug release, and links these directly to their applications in diagnostic imaging (CT, photoacoustic) and combination therapies (PDT, PTT, radiotherapy, chemotherapy, immunotherapy). Finally, it evaluates state-of-the-art nanoplatform designs, addresses clinical challenges, and proposes forward-looking principles to guide the development of clinically impactful Bi_2O_3 theranostic agents.

2. RESULT AND DISCUSSION

2.1. Fundamental Properties of Bismuth Oxide Nanomaterials

Bismuth oxide (Bi_2O_3) is an archetypal polymorphic oxide, and its theranostic potential is tightly coupled to its phase behavior. Bulk Bi_2O_3 exhibits at least five crystallographic polymorphs: monoclinic α-phase stable at room temperature; the tetragonal β-phase; the body-centred cubic γ-phase; the high-temperature cubic δ-phase; and ε-phase [17]. The temperature-dependent phase relations of Bi_2O_3 and the influence of thermal history are summarized schematically in **Fig. 1.**

At low temperature the stable polymorph is α-Bi_2O_3. Upon heating, α-Bi_2O_3 can transform to γ- Bi_2O_3 at around 600 °C, or directly to the high-temperature δ- Bi_2O_3 in the range 710–740 °C. The δ phase represents the precursor to melting: further heating to about 825 °C produces liquid Bi_2O_3. On cooling from the melt, two crystallization paths are possible. Rapid quenching or strong supercooling of the liquid between 825 and 640 °C yields δ-Bi_2O_3, whereas slower cooling favours direct formation of β-Bi_2O_3 from the melt (slow-quench path). Once δ- Bi_2O_3 is formed, it can either convert reversibly to β- Bi_2O_3 on cooling between roughly 775 and 640 °C, or transform to γ- Bi_2O_3 on heating at 635–640 °C; the reverse γ into δ transformation occurs during cooling from 820 down to about 635 °C. The β modification is metastable at low temperature and progressively converts to α- Bi_2O_3 on cooling through approximately 430–640 °C, while δ produced at high temperature transforms back to α- Bi_2O_3 on cooling between 740 and 700 °C. Altogether, the diagram highlights that the polymorph obtained at a given temperature is governed not only by the equilibrium stability fields but also by the heating/cooling direction and the cooling rate, particularly the contrast between rapid quenching and slow quenching from the melt [18-19].

X-ray diffraction (XRD) analysis was employed to identify and distinguish the polymorphic phases of Bi_2O_3 present in the samples. The assignment of diffraction peaks was carried out by comparing the experimental 2θ

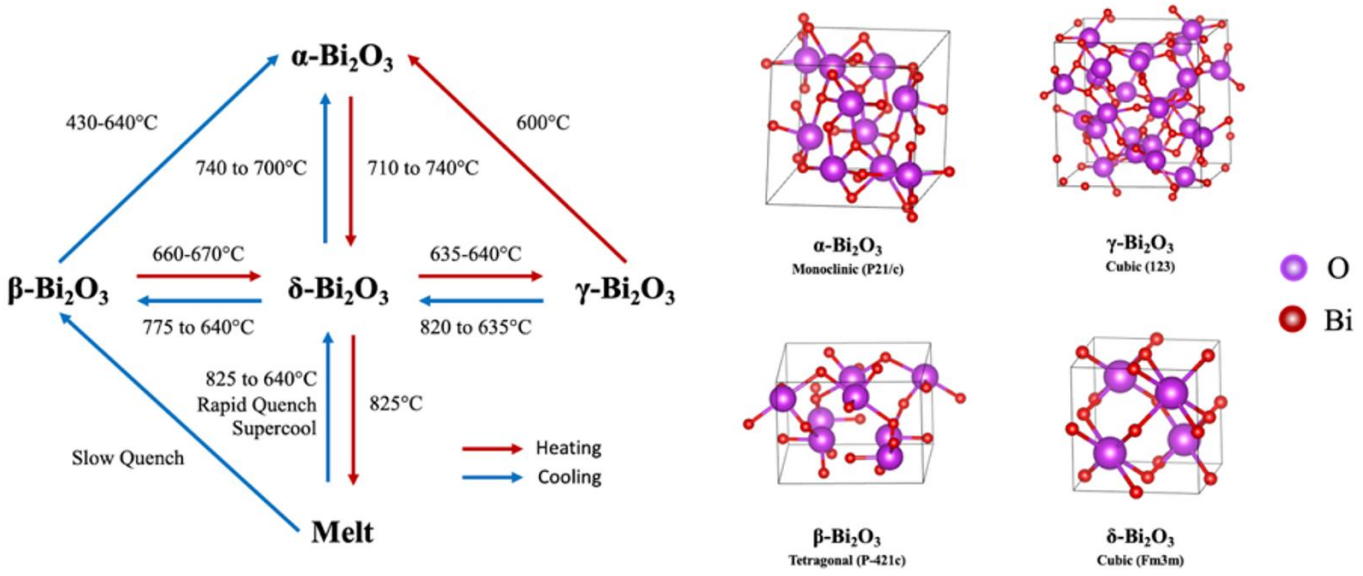

Fig. 1 Schematic representation of the polymorphic transformations and crystal lattice structures of Bi_2O_3

positions with standard reference patterns from the International Centre for Diffraction Data (ICDD), focusing on the most commonly reported cards for α-, β-, γ-, and δ-Bi_2O_3. In particular, the monoclinic α-phase was matched against ICDD PDF 41-1449, the tetragonal β-phase against PDF 27-0050, the cubic γ-phase against PDF 71-0467, and the fluorite-type cubic δ-phase against PDF 52-1007, in accordance with previously published reports. Characteristic reflections for each phase and their corresponding Miller indices (hkl) are summarized in **Table 1**, together with representative literature sources that explicitly reference these ICDD cards. This compilation was used as a guideline for phase identification and to ensure consistent indexing of the diffraction patterns throughout this work.

At the nanoscale, phase stability becomes highly tunable. Polymorph engineering is critical for theranostics nanoplatforms because different phases α vs β yield distinct surface energies, facet exposures, and oxygen-vacancy densities, all of which influence photocatalytic efficiency and ROS generation profiles [27]. Thus, polymorph engineering offers direct control to balance light absorption, catalytic activity, and structural robustness.

The electronic structure of Bi_2O_3 is dominated by the Bi^{3+} $6s^2$ "lone-pair" electrons strongly hybridized with O 2p orbitals in the valence band (VB) and Bi 6p states in the conduction band (CB) [28]. This electronic arrangement produces a moderate band gap of 2.1–2.8 eV [29]. enabling efficient absorption of visible light and thus, photocatalysis. The combination of a moderate band gap and deep VB levels makes Bi_2O_3 an intrinsically powerful visible-light photocatalyst [30].

Upon photoexcitation, electron–hole pairs are generated [31]. The VB holes oxidize water to produce highly reactive hydroxyl radicals (•OH), while CB electrons reduce dissolved oxygen (O_2) to form superoxide radicals ($O_2^{\bullet-}$), initiating a cascade of ROS species (**Fig. 2**). This ROS-driven oxidative stress is directly exploited in cancer theranostics to induce tumor-cell apoptosis.

Photocatalytic performance is strongly phase- and defect-dependent. Oxygen vacancies (Vo) play a dual role, meaning they can act as electron traps that suppress recombination or as excessive non-radiative recombination centers. The formation of heterojunctions (Z-scheme or S-scheme) between Bi_2O_3 and other

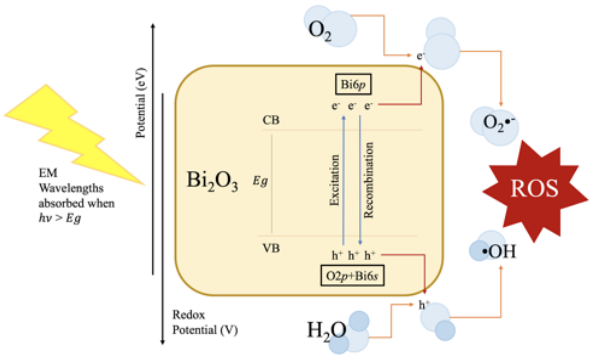

Fig. 2 Schematic representation of ROS generation by Bi_2O_3 light activated

Table 1. Summary of characteristic X-ray diffraction (XRD) reflections used for phase identification of Bi_2O_3 polymorphs based on commonly cited ICDD/PDF cards (Cu Kα, λ = 1.5406 Å)

Phase	Crystal system (space group)	Main ICDD / PDF card(s)	Characteristic 2θ peaks (°) and (hkl)* – Cu Kα	Remarks	References
α-Bi_2O_3	Monoclinic (P21/c)	41-1449 (also 71-0465, 76-1730 for similar data)	~27.3° (120); 32.9–33.0° (200 / –121 / 040); 46.3° (041); 52.1° (321); 54.6–55.5° (241 / –222)	Thermodynamically stable phase at room temperature; widely reported in photocatalysis and oxide ceramics. These reflections are routinely used to confirm monoclinic α-Bi_2O_3 in agreement with the referenced PDF card.	[20-21]
β-Bi_2O_3	Tetragonal (P-421c)	27-0050 (also 78-1793)	~27.9° (201); 31.7° (002); 32.7° (220); 46.2° (222); 46.9° (400); 54.2° (203); 55.5° (421); 57.8° (402); 74.5° (610)	Metastable polymorph typically obtained at elevated temperatures or via solution combustion / nano structuring. The peak set above is frequently indexed to tetragonal β-Bi_2O_3 using PDF 27-0050 in the literature.	[22]
γ- Bi_2O_3	Cubic, body-centred (I23)	71-0467 (also 45-1344)	~12.2° (110); 17.3° (200); 27.4° (310); 30.1° (222); 41.2° (332)	High-temperature cubic polymorph that can be stabilised in nanostructures or doped systems. The low-angle reflections at ~12.2° and 17.3° are particularly distinctive for γ- Bi_2O_3 and are commonly matched to PDF 71-0467.	[23-24]
δ- Bi_2O_3	Cubic fluorite-type (Fm-3m)	52-1007	~27.8–28.0° (111); 32.3° (200); 44.5–46.3° (220); 55.0° (311); 57.6° (222); 67.6° (400); 74.6° (331); 76.9° (420)	High-temperature cubic polymorph that can be stabilised in nanostructures or doped systems. The low-angle reflections at ~12.2° and 17.3° are particularly distinctive for γ- Bi_2O_3 and are commonly matched to PDF 71-0467. studies.	[25-26]

*All 2θ values are approximate and may vary slightly between reports due to instrumental calibration, strain, crystallite size effects, and compositional variations (e.g., dopants).

semiconductors (e.g., $Bi_2O_2CO_3$, Bi_2S_3, or other Bi-oxides) is widely explored to spatially separate electrons and holes while retaining strong redox potential [32]. Furthermore, the high-Z Bismuth nucleus (Z=83) efficiently absorbs X-rays, generating secondary electrons that can also populate the CB pathways responsible for ROS production. This feature bridges classical photocatalysis and radiosensitization in a single nanoplatform.

Every theranostic agent must combine strong physical functionality with acceptable safety [33]. Bi_2O_3 nanomaterials inherit the relatively low systemic toxicity of bulk bismuth [34], exhibiting good cellular uptake and chemical stability [35]. The material's high density and structural robustness support strong CT contrast, often superior to clinical iodine agents at comparable concentrations [36]. Biocompatibility is enhanced through engineering: surface coatings and ligands (such as PAA or cyclodextrins) improve colloidal stability, mitigate off-target toxicity, and enable tumor targeting [37-38].

From a physicochemical perspective, the high density and structural robustness of Bi_2O_3 support strong CT contrast, but may also predispose them to long-term accumulation if not appropriately designed. Therefore, "safe-by-design" frameworks emphasize controlling particle size for renal clearance/metabolism and systematically mapping in vivo [16,39].

Collectively, these features demonstrate Bi_2O_3 as a platform that can be broadly engineered across crystallographic phase, band structure, defect chemistry, and surface state. **Table 2** summarizes these fundamental attributes for the major Bi_2O_3 polymorphs and nanostructured forms, serving as a design map for selecting and tailoring specific Bi_2O_3 phases to meet distinct requirements in imaging, ROS therapy, and radiosensitization of cancer.

2.2. Engineering and Fabrication of Bi_2O_3-Based Nanoplatform

The engineering of Bi_2O_3 nanoplatforms for cancer theranostics requires controlling chemistry across scales, from solution-phase coordination and Bi redox states to crystallization, defect formation, and interfacial assembly. Synthetic route, precursor speciation, nucleation–growth kinetics, and post-synthetic modifications determine phase composition, morphology, surface chemistry, band alignment, and defect density [43]. These structural factors regulate essential theranostic functions, including X-ray attenuation, charge separation, ROS generation, drug loading/release, and in vivo behavior [44]. **Table 3** outlines representative engineering strategies and their

Table 2. Representative fundamental properties of Bi_2O_3 polymorphs relevant to photocatalytic theragnostics

Polymorph / form	Crystal system (bulk)	Typical stability range (bulk)[†]	Representative band gap (eV)[*]	Key features for theragnostics	References
α-Bi_2O_3	Monoclinic	Stable at room temperature; transforms to δ above ~730 °C	~2.4 eV (visible-light active)	Baseline phase; good chemical stability, strong oxidation ability, widely used in photocatalysis and as a building block in heterojunctions.	[40]
β-Bi_2O_3	Tetragonal	Metastable, typically obtained on cooling from high T or via controlled calcination	~2.3–2.8 eV (similar to or slightly higher than α)	Often shows distinct morphology and surface energetics; useful for tuning charge separation and constructing phase-junction photocatalysts.	[13]
γ-Bi_2O_3	Body-centred cubic	Metastable; can be stabilized at RT in nanostructures or via specific annealing pathways	~2.9 eV (phase- and size-dependent)	High symmetry and abundant defect sites favour visible-light absorption and can boost photocatalytic and ROS-generation efficiencies.	[41]
δ-Bi_2O_3	Cubic (fluorite-type, oxygen-deficient)	Classically stable only at high T in bulk; nanostructuring and chemical routes can stabilize δ-like phases at low T	~2.0 eV (strong visible-light response)	High oxide-ion conductivity and rich oxygen-vacancy chemistry; promising for high-activity photocatalysts and defect-engineered radiosensitizers.	[14]
ε-Bi_2O_3	Ordered derivative related to α/β	Accessible via hydrothermal or specialized routes; converts to α around ~400 °C	Insulating, with relatively wide gap (exact value system-dependent)	Ordered structure with low ionic conductivity; may serve as a stable host in composite or core–shell designs.	[42]
Nanostructured Bi_2O_3 (various phases, doped/defective)	Phase-mixed or engineered	Stabilized by size, doping, and heterojunction formation	Typically 1.67–2.86 eV; tunable via phase, size, and dopants	Morphology, vacancy engineering, and band-structure tuning enable optimized ROS generation, photothermal response, and imaging contrast in cancer theranostic systems.	[19]

Table 3. Representative engineering strategies for Bi_2O_3-based nanoplatforms and their structural/functional consequences relevant to cancer theragnostics

Engineering dimension	Representative methods / systems	Key structural and electronic outcomes	Implications for cancer theragnostics	References
Synthetic route and phase/morphology control	Hydrothermal / solvothermal synthesis of α-Bi_2O_3 nanowires, nanosheets, and hierarchical nanoflakes from Bi^{3+} salts; microwave-assisted hydrothermal formation of monoclinic Bi_2O_3 nanorods	Phase-pure α/β- Bi_2O_3 with controlled crystallite size; 1D/2D morphologies with high crystallinity, tailored facet exposure, and tunable defect density	High cristallinity enhance light absorption and charge transport; increased catalytic surface area for ROS generation; abundant surface for drug/ligand attachment and tumour-microenvironment interactions.	[45-46]
Organic-phase core–shell engineering	One-pot thermal decomposition of $Bi(NO_3)_3$ in oleic acid/oleylamine followed by PAA ligand exchange to yield ultrasmall Bi/ Bi_2O_3@PAA NPs	Ultrasmall core–shell particles (≈3–4 nm) with high Bi loading, controlled Bi^0/Bi^{3+} ratio, and dense polymer corona	Ultrasmall morphology resulting in superior CT contrast compared with iodine; potential renal clearance; simultaneous exploitation of high-Z Bi for radiosensitization and Bi_2O_3 for photocatalytic/chemodynamic ROS generation.	[36]
Biomorphic / hierarchical architectures	Pollen-templated Ce-doped porous Bi_2O_3; template-based oxide replicas using sporopollenin exine capsules	Highly porous, interconnected frameworks with large surface area, embedded dopants, and rich oxygen-vacancy networks	High loading capacity because of high porosity for drugs and biomolecules; efficient diffusion of substrates (O_2, H_2O_2, GSH) and products; enhanced photon trapping and ROS production for photodynamic / chemodynamic therapy.	[47]
Surface functionalization and ligand chemistry	PAA- or d-glucuronic acid-coated ultrasmall Bi/ Bi_2O_3 or Bi_2O_3 NPs; β-cyclodextrin-polymer and PDA coatings enabling drug loading and targeting	Hydrophilic, colloidally stable particles with defined zeta potential; functional groups (carboxylates, catechols, cyclodextrin cavities) for PEGylation, targeting ligand conjugation, and drug encapsulation	Improved biocompatibility and blood circulation; reduced off-target accumulation; controlled delivery of chemotherapeutics and radiosensitizers; addition of PA/PTT functionalities via PDA shells.	[48-49]
Doping and defect/vacancy engineering	Ce-doped porous Bi_2O_3 pollen photocatalysts; La/Ce-codoped Bi_2O_3; Ru-doped oxygen-vacancy-rich Bi_2O_3 synthesized by Joule heating	Band-gap narrowing; introduction of shallow donor/acceptor levels; increased oxygen-vacancy concentration; formation of local $Bi_2O_3/Bi_2O_{2.x}$ nano-heterojunctions	Band-gap narrowing tends to enhance visible-light and X-ray–induced ROS generation at lower doses; potential to catalyse Fenton-like or chemodynamic reactions in tumours; tunable redox behaviour matched to TME chemistry.	[50-51]
Binary heterojunctions	β-Bi_2O_3/TiO_2 nanoflower heterojunctions; p–n Bi_2O_3 /TiO_2 photocatalysts; ($Bi_2O_3/Bi_2O_{2.33}$)/TiO2 S-scheme composites	Staggered or S-scheme band alignments with strong internal electric fields; efficient spatial separation of electrons and holes; extended spectral response	Higher ROS yields under optical/ultrasonic/X-ray triggering; improved dose efficiency in radiotherapy and sonodynamic therapy; robust platforms for integrating CT/PA imaging with PDT/RT.	[52-54]
Multicomponent heterojunctions in theranostic platforms	Bi_2O_3–TiO_2 heterojunction cores encapsulated in PDA and loaded with doxorubicin (BTPD) for triple-modality cancer theranostics	Nanoscale heterojunction enabling sonodynamic and photocatalytic ROS production; PDA shell providing PA contrast and drug-loading capacity; DOX as chemotherapeutic cargo	Single-platform integration of CT/PA imaging, sonodynamic therapy, radiosensitization, photothermal contribution, and chemotherapy; exemplifies how Bi_2O_3 engineering interfaces directly with clinical theranostic functions.	[55]

structure–function relationships, serving as a design map for linking synthetic controls to theranostic performance.

Most Bi_2O_3 nanostructures are synthesized through bottom-up wet-chemical routes based on controlled hydrolysis and condensation of Bi^{3+} salts under tuned pH, temperature, and mineralizer conditions [56]. Hydrothermal and solvothermal methods enable precise control of supersaturation and growth, yielding 1D/2D morphologies such as nanowires, nanorods, and nanosheets with high crystallinity [57]. Single-crystalline α-Bi_2O_3 nanowires and nanosheets show enhanced photocatalytic activity due to efficient charge transport and abundant exposed active sites. Microwave-assisted hydrothermal synthesis accelerates nucleation, producing α-Bi_2O_3 nanorods with narrow size distribution [58-59]. Such anisotropic structures offer high surface area, short carrier-diffusion paths, and strong light

scattering, supporting improved ROS generation and drug-conjugation capacity [60].

Organic-phase thermal decomposition is effective for producing ultrasmall Bi-rich nanostructures for imaging. One-pot decomposition of $Bi(NO_3)_3$ in oleic acid/oleylamine forms Bi/Bi_2O_3@PAA nanoparticles (~3 nm cores) with high Bi content, stability, and low cytotoxicity [36]. These particles show superior CT attenuation compared to iodine agents. Ultrasmall Bi_2O_3 nanoparticles coated with d-glucuronic acid similarly provide strong CT contrast and good biocompatibility [48-49]. More advanced systems use β-cyclodextrin–coated Bi_2O_3 nanoparticles modified with glucose and loaded with curcumin, functioning as CT contrast agents, drug carriers, and radiosensitizers.

Morphology-driven strategies, such as sol–gel and hydrothermal preparation of hierarchical nanoflakes and nanosheets, produce porous networks with high surface area and improved visible-light photocatalytic activity [46,48]. Biomorphic templating, exemplified by Ce-doped Bi_2O_3 pollen replicas, creates highly porous architectures with distributed dopants and oxygen vacancies, supporting enhanced ROS generation and drug-loading capacity [47,61]. Hollow and core–shell Bi_2O_3 structures follow similar principles by providing interior voids, defect-rich shells, and enhanced optical path length [62].

Surface functionalization is crucial for biological translation. Carboxylated polymers such as PAA strongly bind surface Bi^{3+}, improving stability, zeta potential, hydration, and reducing cytotoxicity[48]. d-Glucuronic acid coatings also yield hydrophilic, biocompatible ultrasmall particles suitable for CT imaging. Advanced ligand shells, polycyclodextrin networks or PDA coatings, add drug-loading capacity, glucose-mediated uptake, NIR absorption, and conjugation [48-49]. In the Bi_2O_3–TiO_2@PDA–DOX (BTPD) system, PDA enhances biocompatibility, drug loading, and PA imaging, while the Bi_2O_3–TiO_2 core supports sonodynamic and X-ray-induced ROS generation [55].

Doping and defect engineering tune the electronic structure and photocatalytic behavior of Bi_2O_3. Incorporating metals (Ru, Fe), rare earths (La, Ce), or non-metals (N, S) narrows the band gap, introduces donor/acceptor states, and enhances charge mobility [51]. Ru-doped Bi_2O_3 prepared by Joule heating shows high oxygen-vacancy concentration and improved charge separation, markedly enhancing photocatalytic ammonia synthesis. Ce-doped porous Bi_2O_3 photocatalysts benefit from Ce^{3+}/Ce^{4+} redox cycling and higher oxygen-vacancy density. In cancer theranostics, such doped systems are valuable for efficient ROS generation under mild light/X-ray doses and for driving chemodynamic reactions.

Homo- and heterojunction architectures further suppress charge recombination and expand theranostic functionality [63]. Bi_2O_3/TiO_2 heterojunctions, including β-Bi_2O_3/TiO_2 nanoflowers, show improved photocatalytic activity due to type-II or S-scheme charge transfer. Deep-eutectic-solvent synthesis allows regulation of Bi oxidation state and sub-oxide content to modulate internal electric fields. 2D/2D $TiO_2Bi_2O_3$ S-scheme heterostructures exhibit strong spectral response and efficient charge separation [64].

These principles extend directly to cancer theranostics. A Bi_2O_3-TiO_2 PDA–DOX heterojunction system enables ultrasound-triggered ROS generation, X-ray radiosensitization, PA imaging, and chemotherapy [65]. Broad reviews highlight that engineered Bi-based heterostructures support multimodal strategies such as radiotherapy–chemodynamic and radio/photo-thermal combination therapy [66]. Ultimately, band alignment, interface quality, and defect chemistry critically dictate ROS production, radiosensitization efficiency, and tumour selectivity.

2.3. Photocatalytic Mechanisms In Cancer

The functional value of Bi_2O_3-based nanoplatforms lies in their ability to convert incident energy such as light, ultrasound, or X-rays into biologically damaging ROS and heat within tumors. These effects arise from photocatalytic and radiocatalytic pathways that include radical generation, photothermal and sonothermal heating, radiosensitization, and stimulus-responsive drug release, all of which depend on Bi_2O_3's band structure and defect chemistry.

Under irradiation, Bi_2O_3 acts as a visible-light semiconductor in which excitation from the O_2p/Bi_6s valence band to the Bi6p conduction band produces electron–hole pairs [67]. At the particle interface, holes oxidize water to •OH while electrons reduce oxygen to O_2•−, leading to secondary ROS such as HO_2• and H_2O_2. EPR and scavenger studies identify •OH and O_2•− as the dominant species [68]. These radicals induce lipid peroxidation, mitochondrial damage, and DNA breaks in cancer cells; thus, Bi_2O_3 systems with optimized carrier separation amplify ROS generation under low light or X-ray doses [69].

Bi_2O_3 primarily supports Type I PDT, producing O_2•− and •OH through electron-transfer pathways [70]. Incorporating organic chromophores enables Type II PDT, as in Bi-TCPP MOFs that generate $^1O_2$ and trigger immunogenic cell death [71]. In hypoxic tumors, doped or heterojunction Bi_2O_3 platforms can favour Type I routes that remain effective despite low O_2 levels [72].

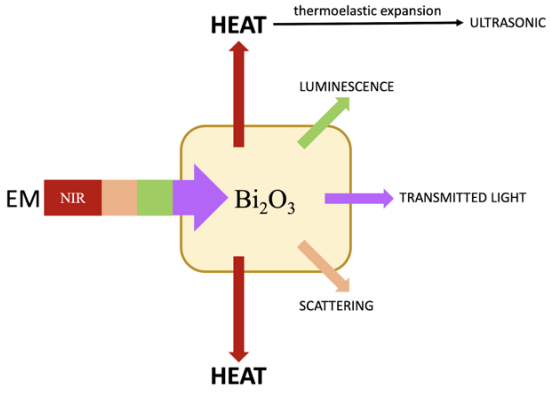

Fig. 3 Schematic representation of ultrasound generation (photoacoustic effect) and heat production (photothermal effect) induced by NIR-activated Bi_2O_3 [74]

Photothermal mechanisms arise from metallic Bi domains, Bi_2O_3-x defects, or Bi chalcogenides, which absorb NIR light and convert it to heat. Bi/Bi_2O_3 core–shell structures show plasmon-like heating and can reach mild hyperthermia under NIR light [73]. Ultrasound also induces heating via acoustic absorption and cavitation, enhanced by oxygen vacancies or metallic components. Hyperthermia improves oxygenation, increases membrane permeability, accelerates radical chemistry, and sensitizes cancer cells (**Fig. 3**) [74]. Therefore, systems combining ROS generation with photo- and sono-thermal heating exploit strong synergy, where heat enhances susceptibility while ROS delivers cytotoxicity.

The radiosensitizing behaviour of Bi_2O_3 anoplatforms arises from the high atomic number of Bi (Z = 83), which enhances photoelectric absorption and secondary-electron production, increasing local ionization and radiolysis yields [75]. This dose amplification improves ROS formation (•OH, e^-aq) and intensifies DNA and lipid damage. Early studies confirmed effective radiosensitization by Bi_2O_3 nanoparticles under X-ray exposure, with later designs incorporating heterostructures such as BP/ Bi_2O_3 hybrids that combine enhanced X-ray absorption, ROS generation, and photothermal contributions. Bi-based RT-CDT systems also use Bi cores to catalyse H2O2 decomposition into •OH, linking radiation dose to catalytic ROS production [76]

Bi_2O_3 enabled photocatalysis and radiothermal effects further support stimulus-responsive drug release. ROS-cleavable linkers, thermosensitive matrices, and partial photocorrosion facilitate controlled payload liberation at irradiated tumour sites [77]. Practical examples include β-cyclodextrin–Bi_2O_3 nanocarriers for curcumin and Bi_2O_3–TiO2@PDA–DOX platforms for combined chemotherapy, sonodynamic therapy, and radiotherapy. Bi-MOFs such as Bi-TCPP also integrate CT/RT enhancement with PDT and immunomodulation [78].

Bismuth-based nanoplatforms increasingly exploit tumour microenvironment (TME) features such as hypoxia, high H202, and elevated GSH [79]. Bi-containing clusters and bismuth oxyhalides generate ROS, deplete GSH, and modulate oxygen balance under radiation or ultrasound. Based on RT-CDT insights, Bi_2O_3 doped with Fe, Cu, or Mn may further catalyse Fenton-like reactions and strengthen multimodal ROS-based therapies [80].

2.4. Theranostic Applications

Theranostic applications of Bi_2O_3 arise from the coupling of its high atomic number (Z=83) for X-ray attenuation, semiconducting properties, and rich surface chemistry with the pathophysiology of solid tumors. A single Bi_2O_3 construct can simultaneously act as a contrast agent for imaging, a photocatalyst for generating reactive oxygen species (ROS) or heat, and a nanocarrier for drugs, enabling integrated "see-and-treat" workflows [81]. **Fig. 4** represents several Bi_2O_3-based nanoplatforms for cancer theranostics.

2.4.1. Diagnostic applications

X-ray CT imaging. Bismuth's high mass attenuation coefficient makes Bi_2O_3 an excellent CT contrast agent, outperforming iodine at lower doses. In hybrid probes like SPIO/ Bi_2O_3/GQDs, the Bi_2O_3 domain provides strong CT contrast. This visibility is used to verify tumor targeting, map radiation dose distribution, and monitor therapy response. For example, CT imaging confirmed the tumor accumulation of β-cyclodextrin-modified Bi_2O_3 nanoparticles loaded with curcumin, guiding effective chemo-radiotherapy [82].

Photoacoustic Imaging. While pure Bi_2O_3 has modest near-infrared (NIR) absorption, oxygen-deficient Bi/Bi_2O_{3-x} heterostructures exhibit strong plasmonic NIR absorption, enabling deep-tissue photoacoustic (PA)

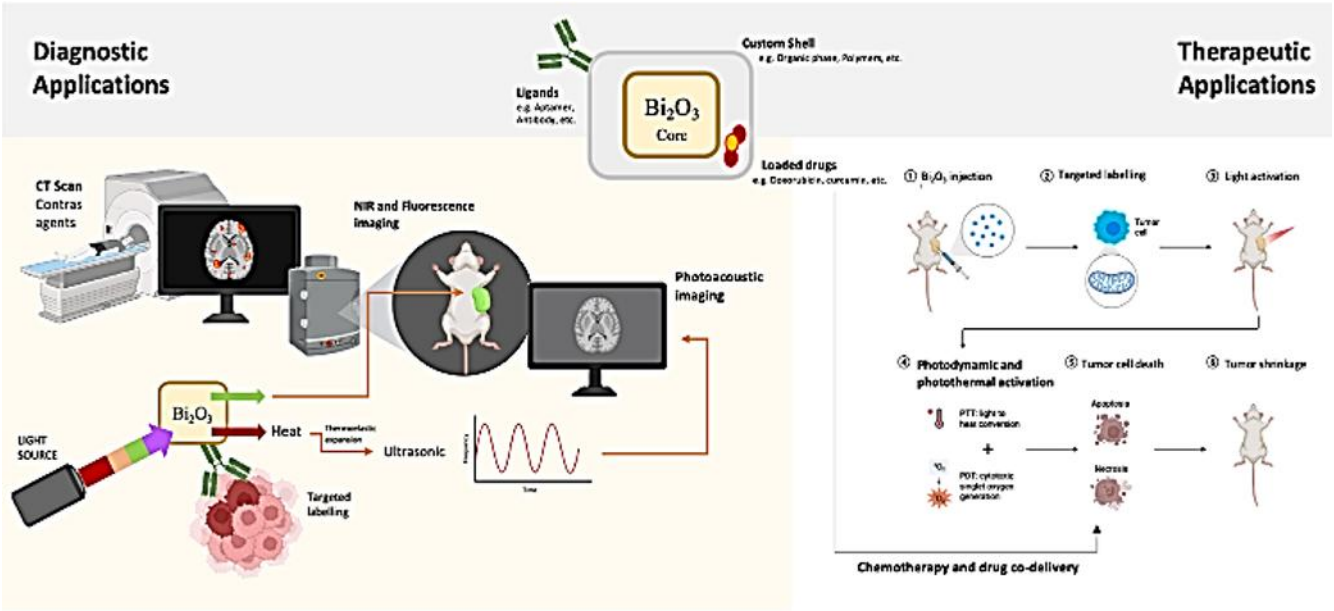

Fig. 4 Bi_2O_3-based nanoplatforms for cancer theranostics [82]

imaging. These nanoparticles allow for visualizing intratumoral distribution and monitoring photothermal therapy (PTT) in real-time. Similarly, Bi_2O_3-TiO_2 nanocages coated with polydopamine (PDA) provide robust PA signals for guiding sonodynamic therapy [83].

Multimodal Imaging. A key strength of Bi_2O_3 is its compatibility with multimodal imaging. Constructs like SPIO/ Bi_2O_3/GQDs offer CT, MRI, and fluorescence imaging in a single platform. The Bi_2O_3-TiO_2-PDA–DOX (BTPD) heterojunction is a prototypical triple-modality agent, providing CT (from Bi), PA (from PDA), and fluorescence (from DOX) for comprehensive image-guided therapy [84].

2.4.2. Therapeutic applications

Photodynamic and Sonodynamic Therapy. Bi_2O_3-based heterostructures can generate ROS under various stimuli. In Bi_2O_3-TiO2 nanoparticles, band alignment facilitates efficient charge separation under ultrasound, boosting ROS production for sonodynamic therapy (SDT) [85]. Bi_2O_3 has also been conjugated with classic photosensitizers like 5-aminolevulinic acid (5-ALA) for conventional photodynamic therapy (PDT). Furthermore, its high-Z nature allows it to act as a radiosensitizer for X-ray-induced PDT (X-PDT), enabling deep-tissue treatment.

Photothermal Therapy. Plasmonic Bi/Bi_2O_3-x nanoparticles show broad NIR absorption and efficient photothermal conversion. Under NIR laser irradiation, these platforms can raise intratumoral temperatures to 42–45 °C, achieving significant tumor ablation, especially when combined with radiotherapy [86].

Radiotherapy Enhancement. Bi_2O_3 is a potent radiosensitizer. Proof-of-concept studies demonstrated that Bi2O3 nanoparticles sensitize radioresistant cells to X-rays, and subsequent work optimized nanorod geometry for enhanced cell killing [87]. In platforms like BTPD, Bi_2O_3 enhances physical dose deposition and contributes to ROS generation, creating powerful combination therapies [88].

Drug Delivery and Immunotherapy. Bi_2O_3's high surface area allows for efficient drug loading. Chitosan-decorated Bi_2O_3 nanoparticles co-delivering curcumin and 5-ALA enable combined chemo-PDT-RT [86]. Furthermore, the ROS and heat generated by Bi_2O_3 platforms can induce immunogenic cell death (ICD), priming the immune system. When combined with checkpoint inhibitors, these systems can convert "cold" tumors into "hot," immunologically active ones [89].

2.5. Recent Advances in Nanoplatform Design

2.5.1. Bandgap-engineered heterostructures

To overcome Bi_2O_3's fast electron-hole recombination, heterojunctions with semiconductors like TiO_2 are constructed. These structures promote charge separation, enhancing ROS yields under clinical stimuli. The BTPD platform is a prime example, integrating sonodynamic therapy, radiotherapy, and chemotherapy [69].

2.5.2. Oxygen-vacancy engineering

Introducing oxygen vacancies into Bi_2O_3 creates defect levels that broaden light absorption and act as electron traps, boosting photocatalytic and photothermal efficiency. Sulfur-doped Bi_2O_3 with abundant VO shows enhanced ROS production and glutathione depletion, a strategy directly applicable to modulating the tumor microenvironment [90].

2.5.3. Smart and stimuli-responsive systems

Bi_2O_3 platforms are being engineered to respond to tumor-specific cues like acidic pH, high glutathione (GSH), and elevated H2O2. For instance, β-cyclodextrin-coated Bi_2O_3 nanoparticles loaded with curcumin leverage glucose for targeting and release their payload in response to the tumor's redox environment, ensuring specific activation at the disease site [91].

2.6. Clinical Prospects and Challenges

The rapid evolution of Bi_2O_3 nanoplatforms makes them compelling candidates for next-generation CT contrast agents and theranostic tools, combining high X-ray attenuation, tunable properties, and a historically favorable biocompatibility profile . Preclinical studies confirm they provide strong CT contrast at lower doses than iodinated agents, and small-molecule Bi-chelates offer a safer, more controllable alternative, building regulatory familiarity.

However, nanoscale safety is complex. "Safe-by-design" analyses emphasize that uncontrolled size, surface chemistry, and crystallinity can lead to long circulation times, RES accumulation, and slow biodegradation, raising concerns about chronic toxicity [92]. A key clinical advantage is their inherent compatibility with existing CT and radiotherapy infrastructure, requiring no hardware modifications. Bi_2O_3 platforms align with precision oncology, enabling molecular targeting and responsiveness to the tumor microenvironment (e.g., hypoxia, pH) [36]. For clinical translation, rigorous control of physicochemical properties, GMP synthesis, and comprehensive long-term toxicity studies are non-negotiable. The most realistic path to the clinic is the stepwise evolution of simplified, well-defined systems that demonstrate clear benefit over existing agents, rather than highly complex constructs [76]. **Table 4** summarized the Advantages and disadvantages of Bi_2O_3 as a cancer theragnostic agent.

3. CONCLUSION

Bismuth oxide (Bi_2O_3) nanoplatforms are advanced theranostic agents that combine high-contrast CT imaging with multimodal cancer therapies, including enhanced radiotherapy and photocatalytic treatments like PDT and PTT. Their functionality can be finely tuned by engineering their polymorphs, defects, and heterojunctions. However, their path to the clinic is hindered by significant challenges in long-term biosafety, biodegradation, and regulatory standardization. For successful translation, a "safe-by-design" approach is

Table 4. Advantages and disadvantages of Bi_2O_3 as a cancer theragnostic agent

Aspect	Advantages of Bi_2O_3	Disadvantages / Challenges of Bi_2O_3
Atomic number and radiodensity	Very high atomic number (Z = 83) enables strong X-ray attenuation and excellent CT contrast; efficient radiosensitization through enhanced photoelectric and Compton interactions at clinical energies.	High-Z nature raises concerns about long-term retention and cumulative dose if particles are not efficiently cleared; careful dose optimization and biodistribution control are required.
Photocatalytic and ROS-generating properties	Visible-light–active semiconductor with tunable bandgap enabling photocatalytic ROS generation for photodynamic-/sonodynamic-like therapy and chemodynamic enhancement.	Intrinsic electron–hole recombination and limited NIR absorption necessitate bandgap/defect engineering or heterojunction design; uncontrolled ROS may damage healthy tissues if targeting and activation are not tightly regulated.
Multimodal theranostic integration	Single platform can combine CT imaging, radiotherapy enhancement, photocatalysis (PDT/SDT), photothermal effects (with suitable composites), and drug delivery for truly multimodal theragnostics.	Increasing structural and compositional complexity complicates manufacturing, quality control, regulatory evaluation, and mechanistic attribution in vivo.
Chemical versatility and structural tunability	Multiple polymorphs, morphologies (nanorods, nanosheets, hollow/porous structures) and heterostructures (with TiO_2, BiOCl, Bi_2S_2, carbon, etc.) allow fine-tuning of optical, electronic, and catalytic properties.	Extensive design space makes it difficult to standardize “lead” formulations; small synthetic variations can significantly alter biodistribution, stability, and safety profiles.
Biocompatibility compared with other heavy metals	Bismuth is generally less toxic than many other high-Z metals; bismuth compounds are already used clinically (e.g., in gastrointestinal medications), supporting a favorable baseline biocompatibility.	Nanoparticulate Bi_2O_3 may show different toxicity, immunogenicity, and long-term accumulation behavior than molecular bismuth drugs; chronic toxicity, immunotoxicity, and excretion must be rigorously characterized.
Tumor microenvironment modulation	With appropriate defect and compositional engineering, Bi_2O_3-based platforms can act as nanozymes and catalytic centers (e.g., for RT–CDT), amplifying ROS within the tumor and depleting antioxidants such as GSH.	Strong catalytic activity can exacerbate off-target oxidative stress if particles distribute to non-tumor tissues; TME heterogeneity may cause highly variable responses between patients and tumor sites.
Compatibility with existing clinical infrastructure	Readily integrates with standard CT and radiotherapy hardware; can be combined with widely available NIR lasers and ultrasound devices for image-guided multimodal therapy.	Clinical implementation still requires new protocols, treatment planning algorithms, and standardized dosing schemes; training and workflow integration are non-trivial.

critical, focusing on simplified, mechanism-driven platforms that integrate seamlessly with existing clinical infrastructure to enable precise and personalized cancer treatment.

4. AUTHOR’S DECLARATION

4.1. Supporting Information

All data generated or analyzed during this review are included in this published article.

4.2. Acknowledgements

The authors thank the Graduate School, Universitas Padjadjaran for providing the institutional support that facilitated this research.

4.3. Conflict of Interest

The authors declare that they have no known competing financial interests or personal relationships that could have appeared to influence the work reported in this paper.

4.4. Author Contributions

The work presented in this review article was collaboratively executed by the authors. RN led the conceptualization, methodology, and original drafting of the manuscript, and was also responsible for the final writing. WIT contributed to literature searching and manuscript editing. LPH and SA provided supervision, contributed to writing–review, and supported data acquisition for the review.

4.5. AI Statement

ChatGPT was utilize to enhance the clarity, grammar, and overall readability of this manuscript. All technical content, data interpretation, and conclusion were solely developed and verified by the authors. The final version of the manuscript was thoroughly reviewed to ensure accuracy, coherence, and aligment with the study’s findings.

5. REFERENCES

[1] American Cancer Society. 2024. *Global Cancer Facts and Figures*.

[2] Imtiaz, S., Ferdous, U.T., Nizela, A., Hasan, A., Shakoor, A., Zia, A.W. and Uddin, S. 2025. Mechanistic study of cancer drug delivery: Current techniques, limitations, and future prospects. *Eur. J. Med. Chem. 290*. 117535. Doi: https://doi.org/10.1016/j.ejmech.2025.117535

[3] Zafar, A., Khatoon, S., Khan, M.J., Abu, J. and Naeem, A. 2025. Advancements and limitations in traditional anti-cancer therapies: A comprehensive review of surgery, chemotherapy, radiation therapy, and hormonal therapy. *Discov. Oncol. 16*(1). 607. Doi: https://doi.org/10.1007/s12672-025-02198-8

[4] Shah, S. and D'Souza, G.G.M. 2025. Modeling tumor microenvironment complexity *in vitro*: Spheroids as physiologically relevant tumor models and strategies for their analysis. *Cells. 14*(10). 732. Doi: https://doi.org/10.3390/cells14100732

[5] Sergeeva, O.V., Luo, L. and Guiseppi-Elie, A. 2025. Cancer theragnostics: Closing the loop for advanced personalized cancer treatment through the platform integration of therapeutics and diagnostics. *Front. Bioeng. Biotechnol. 12*. 1499474. Doi: https://doi.org/10.3389/fbioe.2024.1499474
[6] Mousavi-Kiasary, S.M.S., S.M.S., Senabreh, A., Zandi, A., Pena, R., Cruz, F., Adibi, A. and Hooshmand, N. 2025. Synergistic cancer therapies enhanced by nanoparticles: Advancing nanomedicine through multimodal strategies. *Pharmaceutics. 17*(6). 682. Doi: https://doi.org/10.3390/pharmaceutics17060682
[7] Mutreja, I., Maalej, N., Kaushik, A., Kumar, D. and Raja, A. 2023. High atomic number nanoparticles to enhance spectral CT imaging aspects. *Mater. Adv. 4*(8). 3967–3988. Doi: https://doi.org/10.1039/D3MA00231D
[8] Huang, S.D. 2016. Bismuth-based nanoparticles for CT imaging. *Des. Appl. Nanoparticles Biomed. Imaging.* 429-444. Doi: https://doi.org/10.1007/978-3-319-42169-8_20
[9] Yang, C., Guo, C., Guo, W., Zhao, X., Liu, S. and Han, X. 2018. Multifunctional bismuth nanoparticles as theranostic agent for PA/CT imaging and NIR laser-driven photothermal therapy. *ACS Appl. Nano Mater. 1*(2). 820–830. Doi: https://doi.org/10.1021/acsanm.7b00255
[10] Astuti, Y., Amri, D., Widodo, D.S., Widiyandari, H., Balgis, R. and Ogi, T. 2020. Effect of fuels on the physicochemical properties and photocatalytic activity of bismuth oxide synthesized using solution combustion method. *Int. J. Technol. 11*(1). 26–36. Doi: https://doi.org/10.14716/ijtech.v11i1.3342
[11] Murthy, R.K., Shivanna, M., Ahamed, N.N., Bhoomika, V., Ravikumar, C.R. and Murthy, H.A. 2024. Photocatalytic and electrochemical sensor study of combustion synthesized bismuth oxide (Bi_2O_3) nanoparticles using lemon and urea fuels. *Mater. Sci. Eng. B. 307*. 117487. Doi: https://doi.org/10.1016/j.mseb.2024.117487
[12] Chen, L., Zhang, J., Xu, L., Zhu, L., Jing, J., Feng, Y., Wang, Z., Liu, P., Sun, W., Liu, X. and Li, Y. 2022. Composition tunability of semiconductor radiosensitizers for low-dose X-ray induced photodynamic therapy. *J. Nanobiotechnol. 20*(1). 293. Doi: https://doi.org/10.1186/s12951-022-01494-7
[13] Sharaf, I.M., Koubisy, M.S.I., Alkallas, F.H., Trabelsi, A.B.G. and Aboraia, A.M. 2025. Tailoring β-Bi_2O_3 nanoparticles via Mg doping for superior photocatalytic activity and hydrogen evolution. *Catalysts. 15*(6). Doi: https://doi.org/10.3390/catal15060519
[14] Huang, H., He, L., Zhou, W., Qu, G., Wang, J., Yang, N., Gao, J., Chen, T., Chu, P.K. and Yu, X.F. 2018. Stable black phosphorus/Bi2O3 heterostructures for synergistic cancer radiotherapy. *Biomaterials. 171*. 12-22. Doi: https://doi.org/10.1016/j.biomaterials.2018.04.022
[15] Xiao, F., Liu, Y., Su, Y., He, X., Lu, L., Zhan, M., Wen, L., Dai, Y. and Liu, B. 2024. Biodegradable poly(amino acid)-bismuth nanotheranostic agents for CT/MR imaging and photothermal-chemodynamic synergistic therapy. *Chem Bio Eng. 1*(5). 448–460. Doi: https://doi.org/10.1021/cbe.4c00078
[16] Zhang, X., Gao, F., Dai, Y., Wang, M. and Liu, J. 2025. Safe-by-design strategies towards bismuth-based nanomaterials in tumor diagnosis and therapy. *Nano Today. 62*. 102714. Doi: https://doi.org/10.1016/j.nantod.2025.102714
[17] Amika, Kumar, R., Sharma and Sindhu, M. 2023. Structural and morphological properties of bismuth oxide nanostructured materials. *AIP Conf. Proc. 2008*(1). 020056. Doi: https://doi.org/10.1063/5.0162786
[18] Bartoli, M., Jagdale, P. and Tagliaferro, A. 2020. A short review on biomedical applications of nanostructured bismuth oxide and related nanomaterials. *Materials. 13*(22). 1–17. Doi: https://doi.org/10.3390/ma13225234
[19] Utami, B.A., Sutanto, H., Hidayanto, E. and Alkian, I. 2022. Recent advances in doped Bi_2O_3 and its photocatalytic activity: A review. *Int. J. Res. Rev. 9*(1). 216–230. Doi: https://doi.org/10.52403/ijrr.20220128
[20] Malligavathy, M. and Pathinettam Padiyan, D. 2021. Role of pH in the hydrothermal synthesis of phase pure alpha Bi_2O_3 nanoparticles and its structural characterization. *Adv. Mater. Proc. 2*(1). 51–55. Doi: https://doi.org/10.5185/amp.2017/112
[21] Seswai, K.S., Makola, L.C., Mabuba, N. and Dlamini, L.N. 2024. Fabrication of a hyphenated S-scheme and Schottky-junction photocatalyst based on a ternary TiNbCTx@α-Bi_2O_3/ZnSe heterostructure with enhanced optical and photoelectrochemical properties. *Surf. Interfaces. 51*. 104766. Doi: https://doi.org/10.1016/j.surfin.2024.104766
[22] Sohail, A., Aalim, M., Ahmad, R., Mir, A., Majeed, A., Shah, M.A. and Majid, K. 2024. Enhanced photocatalytic performance of β-Bi_2O_3 nanospheres under visible light irradiation. *Springer Proc. Mater. 27*. 293–297. Doi: https://doi.org/10.1007/978-981-99-4878-9_41
[23] Iyyapushpam, S., Nishanthi, S.T. and Padiyan, D.P. 2014. Enhanced photocatalytic degradation of methyl orange by γ-Bi_2O_3 and its kinetics. *J. Alloys Compd. 601*. 85–87. Doi: https://doi.org/10.1016/j.jallcom.2014.02.142
[24] Yan, Q., Xie, X., Liu, Y., Wang, S., Zhang, M., Chen, Y. and Si, Y. 2019. Constructing a new Z-scheme multi-heterojunction photocatalysts Ag–AgI/BiOI–Bi_2O_3 with enhanced photocatalytic activity. *J. Hazard. Mater. 371*. 304–315. Doi: https://doi.org/10.1016/j.jhazmat.2019.03.031
[25] Sudrajat, H. and Sujaridworakun, P. 2017. Low-temperature synthesis of δ-Bi_2O_3 hierarchical nanostructures composed of ultrathin nanosheets for efficient photocatalysis. *Mater. Des. 130*. 501–511. Doi: https://doi.org/10.1016/j.matdes.2017.05.087
[26] Chen, Q. and Wang, H. 2020. Tunable optical linear and nonlinear, magnetic and Faraday rotation properties: Comparison of ZnO-based DMS alloys in diamagnetic solid matrix. *J. Alloys Compd. 846*. 156394. Doi: https://doi.org/10.1016/j.jallcom.2020.156394
[27] Cadenbach, T., Loyola-Plúa, M.I., Quijano Carrasco, F., Benitez, M.J., Debut, A. and Vizuete, K. 2025. Controlled formation of α- and β-Bi_2O_3 with tunable morphologies for visible-light-driven photocatalysis. *Molecules. 30*(15). Doi: https://doi.org/10.3390/molecules30153190
[28] Awater, R.H. and Dorenbos, P. 2017. The Bi^{3+} 6s and 6p electron binding energies in relation to the chemical environment of inorganic compounds. *J. Lumin. 184*. 221–231. Doi: https://doi.org/10.1016/j.jlumin.2016.12.021
[29] Mane, V., Dake, D., Raskar, N., Sonpir, R., Stathatos, E. and Dole, B. 2024. A review on Bi_2O_3 nanomaterial for photocatalytic and antibacterial applications. *Chem. Phys. Impact. 8*. 100517. Doi: https://doi.org/10.1016/j.chphi.2024.100517
[30] Prabhakar Vattikuti, S.V., Zeng, J., Ramaraghavulu, R., Shim, J., Mauger, A. and Julien, C.M. 2023. High-throughput strategies for the design, discovery, and analysis of bismuth-based photocatalysts. *Int. J. Mol. Sci. 24*(1). 663. Doi: https://doi.org/10.3390/ijms24010663
[31] Huang, X., Zha, F., Zou, J., Li, Y., Wang, F. and Chen, X. 2022. Photoacoustic imaging-guided synergistic photothermal/radiotherapy using plasmonic Bi/Bi_2O_3−x nanoparticles. *Adv. Funct. Mater. 32*(23). 2113353. Doi: https://doi.org/10.1002/adfm.202113353
[32] Chowdhury, A.P., Anantharaju, K.S., Keshavamurthy, K., Swain, S. and Uma, B. 2025. A mini-review on Z- and S-scheme heterojunction bismuth-based photocatalysts towards H_2 production, CO_2 reduction, and pollutant degradation. *Next Mater. 8*. 100918. Doi: https://doi.org/10.1016/j.nxmate.2025.100918
[33] Azimizonuzi, H., Ghayourvahdat, A., Ahmed, M.H., Kareem, R.A., Zrzor, A.J., Mansoor, A.S., Athab, Z.H. and Kalavi, S. 2025. A state-of-the-art review of the recent advances of theranostic liposome hybrid nanoparticles in cancer treatment and diagnosis. *Cancer Cell Int. 25*(1). 26. Doi: https://doi.org/10.1186/s12935-024-03610-z
[34] Gonçalves, Â., Matias, M., Salvador, J.A.R. and Silvestre, S. 2024. Bioactive bismuth compounds: Is their toxicity a barrier to therapeutic use? *Int. J. Mol. Sci. 25*(3). 1600. Doi: https://doi.org/10.3390/ijms25031600
[35] Dhanasekarana, E., Sivakumarb, N. and Sriharanc, N. 2022. Enhanced photocatalytic degradation of Gd-doped Bi_2O_3 for selective dyes under UV light irradiation. *J. Optoelectron. Biomed. Mater. 14*(3). 77–87. Doi: https://doi.org/10.15251/jobm.2022.143.77
[36] Ganapathy, D., Shivalingam, C., Shanmugam, R., Sundramoorthy, A.K., Murthykumar, K., Pitchiah, S., Sekaran, S. and Ramachandran, S.K. 2022. Recent breakthrough of bismuth-based nanostructured materials for multimodal theranostic applications. *J. Nanomater. 2022*(1). 4944320. Doi: https://doi.org/10.1155/2022/4944320
[37] Alex, J. and Mathew, T.V. 2023. Surface modification of Bi_2O_3 nanoparticles with biotinylated β-cyclodextrin as a biocompatible

therapeutic agent for anticancer and antimicrobial applications. *Molecules.* *28*(8). 3604 Doi: https://doi.org/10.3390/molecules28083604

[38] Khalili, Z., Motakef Kazemi, N., Jafari Azar, Z., Mosavi, Z. and Hasanzadeh, M. 2024. Fabrication and characterization of a Bi_2O_3-modified chitosan@ZIF-8 nanocomposite for enhanced drug loading-releasing efficacy. *Int. J. Biol. Macromol. 263*. 130295. Doi: https://doi.org/10.1016/j.ijbiomac.2024.130295

[39] Sikora, P., El-Khayatt, A.M., Saudi, H.A., Chung, S.Y., Stephan, D. and Abd Elrahman, M. 2021. Evaluation of the effects of bismuth oxide (Bi_2O_3) micro- and nanoparticles on the mechanical, microstructural and γ-ray/neutron shielding properties of Portland cement pastes. *Constr. Build. Mater. 284*. 122758. Doi: https://doi.org/10.1016/j.conbuildmat.2021.122758

[40] Ruiz-Castillo, A.L., Hinojosa-Reyes, M., Camposeco-Solis, R. and Ruiz, F. 2022. Photocatalytic activity of Bi_2O_3/BiOCl heterojunctions under UV and visible light illumination for degradation of caffeine. *Top. Catal. 65*. 1071–1087. Doi: https://doi.org/10.1007/s11244-022-01644-z

[41] Gandhi, A.C., Cheng, C.L. and Wu, S.Y. 2020. Structural and enhanced optical properties of stabilized γ-Bi_2O_3 nanoparticles: Effect of oxygen ion vacancies. *Nanomaterials. 10*(6). 1023. Doi: https://doi.org/10.3390/nano10061023

[42] Cornei, N., Tancret, N., Abraham, F. and Mentré, O. 2006. New ε-Bi_2O_3 metastable polymorph. *Inorg. Chem. 45*(12). 4886–4888. Doi: https://doi.org/10.1021/ic0605221

[43] Ali, F.S., Ragamathunnisa, M., Al Marzouqi, F., Jahangir, A.R.M., Ayeshamariam, A. and Kaviyarasu, K. 2019. Synthesis and characterization of Bi_2O_3 nanoparticles and photocatalytic application with methylene blue. *JOBM. 13*(3), 95-106. Doi: https://doi.org/10.21203/rs.3.rs-577935/v1

[44] Duan, X., Wang, P., He, L., He, Z., Wang, S., Yang, F., Gao, C., Ren, W., Lin, J., Chen, T. and Xu, C. 2024. Peptide-functionalized inorganic oxide nanomaterials for solid cancer imaging and therapy. *Adv. Mater. 36*(37). 2311548. Doi: https://doi.org/10.1002/adma.202311548

[45] Wu, Y.C., Chiang, Y.C., Huang, C.Y., Wang, S.F. and Yang, H.Y. 2013. Morphology-controllable Bi_2O_3 crystals through an aqueous precipitation method and their photocatalytic performance. *Dyes Pigments. 99*(1). 25–30. Doi: https://doi.org/10.1016/j.dyepig.2013.02.006

[46] Al-Ghamdi, A.A., Al-Turki, Y., Aal, N.A., Yakuphanoglu, F. and El-Tantawy, F. 2017. Microwave-assisted hydrothermal synthesis of monoclinic bismuth trioxide nanorods: Optical and photocatalytic properties. *J. Mater. Sci. Mater. Electron. 28*(12). 8684–8693. Doi: https://doi.org/10.1007/s10854-017-6593-3

[47] Kong, S., Zhang, T., He, Y., Zhou, Y., Yan, G. and Huang, M. 2025. Porous Ce-doped Bi_2O_3 pollen biomorphic photocatalyst with high specific surface area and oxygen vacancies for efficient degradation of tetracycline. *J. Rare Earths. 44*(3). 776-790. Doi: https://doi.org/10.1016/j.jre.2025.03.032

[48] Wu, H., Kong, J., Yao, X., Zhao, C., Dong, Y. and Lu, X. 2015. Polydopamine-assisted attachment of β-cyclodextrin on porous electrospun fibers for water purification under highly basic condition. *Chem. Eng. J. 270*. 101–109. Doi: https://doi.org/10.1016/j.cej.2015.02.019

[49] Ghazanfari, A., Marasini, S., Yue, H., Ho, S.L., Miao, X., Ahmad, M.Y., Park, J., Jung, K.H., Liu, S., Jang, Y.J. and Chae, K.S. 2020. D-Glucuronic acid-coated ultrasmall Bi_2O_3 nanoparticles for CT imaging. *J. Nanosci. Nanotechnol. 20*(8). 4638–4642. Doi: https://doi.org/10.1166/jnn.2020.17817

[50] Xue, S., He, H., Fan, Q., Yu, C., Yang, K., Huang, W., Zhou, Y. and Xie, Y. 2017. La/Ce-codoped Bi_2O_3 composite photocatalysts with high photocatalytic performance in removal of high concentration dye. *J. Environ. Sci. 60*. 70–77. Doi: https://doi.org/10.1016/j.jes.2016.09.022

[51] Chu, Q., Ren, G. and Meng, X. 2025. Ru-doped Bi_2O_3 with rich oxygen vacancy for enhanced photocatalytic nitrogen reduction. *J. Alloys Compd. 1012*. 178441. Doi: https://doi.org/10.1016/j.jallcom.2024.178441

[52] Tang, T., Yin, Z., Chen, J., Zhang, S., Sheng, W., Wei, W., Xiao, Y., Shi, Q. and Cao, S. 2021. Novel p–n heterojunction Bi_2O_3/Ti^{3+}-TiO_2 photocatalyst enables the complete removal of tetracyclines under visible light. *Chem. Eng. J. 417*. 128058. Doi: https://doi.org/10.1016/j.cej.2020.128058

[53] Yang, J., Wang, X., Yan, S., Huang, F., Xia, X., Zhao, Y., Hao, P., Cui, G. and Wang, Q. 2025. Facile construction of (Bi_2O_3/$Bi_2O_{2.33}$)/TiO_2 S-scheme heterojunction by deep eutectic solvent-regulated strategy for enhanced photocatalytic tetracycline degradation. *J. Alloys Compd. 1020*. 179400. Doi: https://doi.org/10.1016/j.jallcom.2025.179400

[54] Wang, M., Li, C., Liu, B., Qin, W. and Xie, Y. 2023. Facile synthesis of nano-flower β-Bi_2O_3/TiO_2 heterojunction as photocatalyst for degradation of RhB. *Molecules. 28*(2). 882. Doi: https://doi.org/10.3390/molecules28020882

[55] Zheng, Z., Williams, G.R., Guo, H., Zheng, Y., Xiu, M., Zhang, Y., Zhang, H., Wang, K., Xia, J., Wang, Y. and Zhu, L.M. 2025. A Bi_2O_3-TiO_2 heterojunction for triple-modality cancer theranostics. *Int. J. Nanomedicine. 20*. 5593–5610. Doi: https://doi.org/10.2147/IJN.S511891

[56] Hoff, B.L., Cheng, G., Villalpando, G., Yuan, F., Yao, N. and Schoop, M.L. 2022. Chemically exfoliated nanosheets of β-Bi_2O_3. *JPhys Mater. 5*(4). Doi: https://doi.org/10.1088/2515-7639/ac92a7

[57] Zheng, F.L., Li, G.R., Ou, Y.N., Wang, Z.L., Su, C.Y. and Tong, Y.X. 2010. Synthesis of hierarchical rippled Bi_2O_3 nanobelts for supercapacitor applications. *Chem. Commun. 46*(27). 5021–5023. Doi: https://doi.org/10.1039/C002126A

[58] Yahyazadehfar, M., Sheikhhosseini, E., Ahmadi, S.A. and Ghazanfari, D. 2022. Microwave-assisted synthetic method of novel Bi_2O_3 nanostructure and its application as a high-performance nanocatalyst in preparing benzylidene barbituric acid derivatives. *Front. Chem. 10*. 951229. Doi: https://doi.org/10.3389/fchem.2022.951229

[59] Xiangying, C. and Huh, H.S. 2007. Controlled synthesis of bismuth oxo nanoscale crystals (BiOCl, $Bi_{12}O_{17}Cl_2$, α-Bi_2O_3, and $(BiO)_2CO_3$) by solution-phase methods. *J. Solid State Chem. 180*(9). 2510–2516. Doi: https://doi.org/10.1016/j.jssc.2007.06.030

[60] Johnson, P.M., Bret, B.P.J., Rivas, J.G., Kelly, J.J. and Lagendijk, A. 2002. Anisotropic diffusion of light in a strongly scattering material. *Phys. Rev. Lett. 89*(24). 243901. Doi: https://doi.org/10.1103/PhysRevLett.89.243901

[61] Yang, Z., Shi, C., Cheng, D., Wang, Y., Xing, Y., Du, F., Wu, F., Jin, Y., Dong, Y. and Li, M. 2022. Biomimetic nanomaterial-facilitated oxygen generation strategies for enhancing tumour treatment outcomes. *Front. Bioeng. Biotechnol. 10*. 1007960. Doi: https://doi.org/10.3389/fbioe.2022.1007960

[62] Yan, Y., Chang, K., Ni, T. and Li, K. 2019. L-Cysteine-assisted synthesis of Bi_2S_3 hollow sphere with enhanced near-infrared light harvesting for photothermal conversion and drug delivery. *Mater. Lett. 245*. 158–161. Doi: https://doi.org/10.1016/j.matlet.2019.02.104

[63] Liu, J., Shi, J. and Deng, H. 2023. Current status of research on BiOX-based heterojunction photocatalytic systems: Synthesis methods, photocatalytic applications and prospects. *J. Environ. Chem. Eng. 11*(5). 110311. Doi: https://doi.org/10.1016/j.jece.2023.110311

[64] Abdelkader, S.A., Cui, Z., Laachachi, A., Colbeau-Justin, C. and Ghazzal, M.N. 2021. Interfacial charge transfer and photocatalytic activity in a reverse-designed Bi_2O_3/TiO_2 core-shell. *Front. Energy. 15*(3). 732–743. Doi: https://doi.org/10.1007/s11708-021-0772-x

[65] Wang, Z., Liu, S., Wang, L., Zou, H., Wang, Z., Tang, X., Feng, W., Chong, Y., Liu, Y., Yang, B. and Zhang, H. 2020. $BiVO_4$@Bi_2S_3 heterojunction nanorods with enhanced charge separation efficiency for multimodal imaging and synergy therapy of tumor. *ACS Appl. Bio Mater. 3*(8). 5080–5092. Doi: https://doi.org/10.1021/acsabm.0c00573

[66] Zhao, H., Wang, J., Li, X., Li, Y., Li, C., Wang, X., Wang, J., Guan, S., Xu, Y., Deng, G. and Chen, Y. 2021. A biocompatible theranostic agent based on stable bismuth nanoparticles for X-ray computed tomography/magnetic resonance imaging-guided enhanced chemo/photothermal/chemodynamic therapy for tumours. *J. Colloid Interface Sci. 604*. 80–90. Doi: https://doi.org/10.1016/j.jcis.2021.06.174

[67] Sajjad, S., Leghari, S.A.K. and Zhang, J. 2013. Nonstoichiometric Bi_2O_3: Efficient visible light photocatalyst. *RSC Adv. 3*(5). 1363–1367. Doi: https://doi.org/10.1039/C2RA22239F

[68] Xu, X., Sun, Y., Fan, Z., Zhao, D., Xiong, S., Zhang, B., Zhou, S. and Liu, G. 2018. Mechanisms for $\cdot O_2^-$ and ·OH production on

flowerlike $BiVO_4$ photocatalysis based on electron spin resonance. *Front. Chem. 6*. 64. Doi: https://doi.org/10.3389/fchem.2018.00064

[69] Liu, H., Cheng, R., Dong, X., Zhu, S., Zhou, R., Yan, L., Zhang, C., Wang, Q., Gu, Z. and Zhao, Y. 2020. BiO_2−x nanosheets as radiosensitizers with catalase-like activity for hypoxia alleviation and enhancement of the radiotherapy of tumors. *Inorg. Chem. 59*(6). 3482–3493. Doi: https://doi.org/10.1021/acs.inorgchem.9b03280

[70] Riente, P., Fianchini, V., Llanes, P., Pericàs, M.A. and Noël, T. 2021. Shedding light on the nature of the catalytically active species in photocatalytic reactions using Bi_2O_3 semiconductor. *Nat. Commun. 12*(1). 625. Doi: https://doi.org/10.1038/s41467-020-20882-x

[71] Luo, T., Ni, K., Culbert, A., Lan, G., Li, Z., Jiang, X., Kaufmann, M. and Lin, W. 2020. Nanoscale metal-organic frameworks stabilize bacteriochlorins for type I and type II photodynamic therapy. *J. Am. Chem. Soc. 142*(16). 7334–7339. Doi: https://doi.org/10.1021/jacs.0c02129

[72] Zhen, W., Liu, Y., Jia, X., Wu, L., Wang, C. and Jiang, X. 2019. Reductive surfactant-assisted one-step fabrication of a $BiOI/BiOIO_3$ heterojunction biophotocatalyst for enhanced photodynamic theranostics overcoming tumor hypoxia. *Nanoscale Horiz. 4*(3). 720–726. Doi: https://doi.org/10.1039/C8NH00440D

[73] Fang, C., Ding, Q., Bi, T., Xu, X., Chen, J.L., Zhu, X.M. and Geng, B. 2018. Plasmonic band-tunable (Au nanocrystal)/SnO_2 core/shell hybrids for photothermal therapy. *Part. Part. Syst. Charact. 35*(10). 1800238. Doi: https://doi.org/10.1002/ppsc.201800238

[74] Son, S., Kim, J.H., Wang, X., Zhang, C., Yoon, S.A., Shin, J., Sharma, A., Lee, M.H., Cheng, L., Wu, J. and Kim, J.S. 2020. Multifunctional sonosensitizers in sonodynamic cancer therapy. *Chem. Soc. Rev. 49*(11). 3244–3261. Doi: https://doi.org/10.1039/C9CS00648F

[75] Jay-Gerin, J.P. 2020. Ultra-high dose-rate (FLASH) radiotherapy: Generation of early, transient, strongly acidic spikes in the irradiated tumor environment. *Cancer Radiother. 24*(4). 332–334. Doi: https://doi.org/10.1016/j.canrad.2019.11.004

[76] Aghanwa, C.I., Umoke, N.H., Adanigbo, P., Babatunde, R.O., Fafioye, A.O., Adara, R.J., Ofoka, E.A., Ezennubia, K.P., Erumiseli, O. and Ifijen, I.H. 2025. Radiotherapy-chemodynamic cancer therapy using bismuth-based nanoparticles: A synergistic approach for enhanced cancer treatment. *RSC Adv. 15*(40). 32956–32994. Doi: https://doi.org/10.1039/D5RA03984C

[77] Vasvani, S., Vasukutty, A., Bardhan, R., Park, I.K. and Uthaman, S. 2024. Reactive oxygen species-driven prodrug-based nanoscale carriers for transformative therapies. *Biomater. Sci. 12*(17). 4335–4353. Doi: https://doi.org/10.1039/D4BM00647J

[78] Li, T., Gao, M., Wu, Z., Yang, J., Mo, B., Yu, S., Gong, X., Liu, J., Wang, W., Luo, S. and Li, R. 2023. Tantalum–zirconium co-doped metal-organic frameworks sequentially sensitize radio-radiodynamic-immunotherapy for metastatic osteosarcoma. *Adv. Sci. 10*(10). 2206779. Doi: https://doi.org/10.1002/advs.202206779

[79] Mbugua, S.N. 2022. Targeting tumor microenvironment by metal peroxide nanoparticles in cancer therapy. *Bioinorg. Chem. Appl. 2022*(1). 5041399. Doi: https://doi.org/10.1155/2022/5041399

[80] Liu, J., Zhang, J., Song, K., Du, J., Wang, X., Liu, J., Li, B., Ouyang, R., Miao, Y., Sun, Y. and Li, Y. 2021. Tumor microenvironment modulation platform based on composite biodegradable bismuth–manganese radiosensitizer for inhibiting radioresistant hypoxic tumors. *Small. 17*(34). 2101015 Doi: https://doi.org/10.1002/smll.202101015

[81] Chen, D., Miao, B., Zhu, G., Liang, Y. and Wang, C. 2024. Controllable synthesis and biomedical applications of bismuth-based nanospheres: Enhanced photothermal therapy and CT imaging efficiency. *Nanoscale. 17*(4). 2281–2291. Doi: https://doi.org/10.1039/D4NR04024D

[82] Rajaee, A., Wang, S., Zhao, L., Wang, D., Liu, Y., Wang, J. and Ying, K. 2019. Multifunction bismuth gadolinium oxide nanoparticles as radiosensitizer in radiation therapy and imaging. *Phys. Med. Biol. 64*(19). 195007. Doi: https://doi.org/10.1088/1361-6560/ab2154

[83] Chen, G., Du, J., Gu, L., Wang, Q., Qi, Q., Li, X., Zhang, R., Yang, H., Miao, Y. and Li, Y. 2024. Metal-sensitized Au-Bi_2O_3 nanoheterojunction for immunogenic cell death-boosted sono-immuno cancer therapy. *Chem. Eng. J. 482*. 148953. Doi: https://doi.org/10.1016/j.cej.2024.148953

[84] Ma, S., Xie, J., Wang, L., Zhou, Z., Luo, X., Yan, J. and Ran, G. 2021. Hetero-core-shell BiNS-Fe@Fe as a potential theranostic nanoplatform for multimodal imaging-guided simultaneous photothermal-photodynamic and chemodynamic treatment. *ACS Appl. Mater. Interfaces. 13*(9). 10728–10740. Doi: https://doi.org/10.1021/acsami.0c21579

[85] Yang, Z., Yuan, M., Liu, B., Zhang, W., Maleki, A., Guo, B., Ma, P.A., Cheng, Z. and Lin, J. 2022. Conferring $BiVO_4$ nanorods with oxygen vacancies to realize enhanced sonodynamic cancer therapy. *Angew. Chem. Int. Ed. 61*(44). e202209484. Doi: https://doi.org/10.1002/anie.202209484

[86] Badrigilan, S., Choupani, J., Khanbabaei, H., Hoseini-Ghahfarokhi, M., Webster, T.J. and Tayebi, L. 2020. Bismuth-based nanomaterials: Recent advances in tumor targeting and synergistic cancer therapy techniques. *Adv. Healthc. Mater. 9*(7). 1901695. Doi: https://doi.org/10.1002/adhm.201901695

[87] Du, F., Lou, J., Jiang, R., Fang, Z., Zhao, X., Niu, Y., Zou, S., Zhang, M., Gong, A. and Wu, C. 2017. Hyaluronic acid-functionalized bismuth oxide nanoparticles for computed tomography imaging-guided radiotherapy of tumor. *Int. J. Nanomedicine. 12*. 5973–5992. Doi: https://doi.org/10.2147/IJN.S130455

[88] Ma, Y.C., Tang, X.F., Xu, Y.C., Jiang, W., Xin, Y.J., Zhao, W., He, X., Lu, L.G. and Zhan, M.X. 2021. Nano-enabled coordination platform of bismuth nitrate and cisplatin prodrug potentiates cancer chemoradiotherapy via DNA damage enhancement. *Biomater. Sci. 9*(9). 3401–3409. Doi: https://doi.org/10.1039/D1BM00157D

[89] Wang, S., Chen, W., Jiang, C. and Lu, L. 2019. Nanoscaled porphyrinic metal-organic framework for photodynamic/photothermal therapy of tumor. *Electrophoresis. 40*(16). 2204–2210. Doi: https://doi.org/10.1002/elps.201900005

[90] Mo, D., Pan, M., Chen, W., Liu, Q., Yu, Y., Yuan, L., Yang, Y., Deng, H., Wang, M. and Qian, Z. 2024. Sulfur vacancy-rich Bi_2S_3−x@PDA heterojunctions with light-controlled reactive oxygen species generation and elimination to combat biofilm infection and inflammation caused by drug-resistant bacteria. *Adv. Funct. Mater. 34*(26). 2313569. Doi: https://doi.org/10.1002/adfm.202313569

[91] Ghaffari, S.B., Sarrafzadeh, M.H., Fakhroueian, Z. and Khorramizadeh, M.R. 2019. Flower-like curcumin-loaded folic acid-conjugated ZnO-MPA-β-cyclodextrin nanostructures enhanced anticancer activity and cellular uptake of curcumin in breast cancer cells. *Mater. Sci. Eng. C. 103*. 109827. Doi: https://doi.org/10.1016/j.msec.2019.109827

[92] Szostak, K., Ostaszewski, P., Pulit-Prociak, J. and Banach, M. 2019. Bismuth oxide nanoparticles in drug delivery systems. *Pharm. Chem. J. 53*(1). 48–51. Doi: https://doi.org/10.1007/s11094-019-01954-9